








DDO68 C: The Actual Appearance of a Ghost Satellite Dwarf through Adaptive Optics at the Large Binocular Telescope

Francesca Annibali¹, Enrico Pinna², Leslie K. Hunt² , Diego Paris³ , Felice Cusano¹ , Michele Bellazzini¹ ,
John M. Cannon⁴ , Raffaele Pascale¹, Monica Tosi¹ , and Fabio Rossi²

¹ INAF—Osservatorio di Astrofisica e Scienza dello Spazio, Via Piero Gobetti, 93/3, I-40129 Bologna, Italy; francesca.annibali@inaf.it

² INAF—Osservatorio Astrofisico di Arcetri, Largo Enrico Fermi 5, I-50125 Firenze, Italy

³ INAF—Osservatorio Astronomico di Roma, Via Frascati 33, I-00078 Monte Porzio Catone, Italy

⁴ Macalester College, 1600 Grand Avenue, Saint Paul, MN 55105, USA

Received 2022 September 2; revised 2022 November 27; accepted 2022 December 13; published 2023 January 6

Abstract

Through adaptive optics (AO) imaging with the SOUL+LUCI instrument at the Large Binocular Telescope we were able to resolve, for the first time, individual stars in the gas-rich galaxy DDO68 C. This system was already suggested to be interacting with the extremely metal-poor dwarf DDO68, but its nature has remained elusive so far because of the presence of a bright foreground star close to its line of sight that hampers a detailed study of its stellar population and distance. In our study, we turned this interloper star into an opportunity to have a deeper insight on DDO68 C, using it as a guide star for the AO correction. Although the new data do not allow for a direct distance measurement through the red giant branch tip method, the combined analysis of the resolved-star color-magnitude diagram, of archival GALEX far-UV and near-UV photometry, and of H α data provides a self-consistent picture in which DDO68 C is at the same ~ 13 Mpc distance as its candidate companion DDO68. These results indicate that DDO68 is a unique case of a low-mass dwarf, less massive than the Magellanic Clouds, interacting with three satellites (DDO68 C and two previously confirmed accreting systems), providing useful constraints on cosmological models and a potential explanation for its anomalous extremely low metallicity.

Unified Astronomy Thesaurus concepts: Dwarf galaxies (416); Dwarf irregular galaxies (417); Interacting galaxies (802); Galaxy stellar content (621); Adaptive optics (2281)

1. Introduction

The most metal-poor, star-forming dwarf galaxies in the nearby universe are of paramount importance since they offer the opportunity to study the details of star formation and chemical evolution in a regime similar to that of primordial galaxies in the early universe (e.g., Izotov et al. 1994; Kunth & Östlin 2000; Senchyna et al. 2019; McQuinn et al. 2020; Annibali & Tosi 2022). Extremely metal-poor dwarfs (XMPs), with an oxygen abundance of $12 + \log(\text{O}/\text{H}) \leq 7.35$ or $\lesssim 4\%$ solar (e.g., Guseva et al. 2015), are quite rare galaxies, and because of interest in them, they have been actively sought in recent years by many groups (Pustilnik et al. 2005; Izotov et al. 2012; Skillman et al. 2013; Hirschauer et al. 2016; Guseva et al. 2017; Hsyu et al. 2017; Yang et al. 2017; Hsyu et al. 2018; Senchyna et al. 2019; Kojima et al. 2020; McQuinn et al. 2020; Pustilnik et al. 2021). While some XMPs can be explained with the combined effects of inefficient star formation and high metal loss via galactic winds at low galaxy masses (e.g., Skillman et al. 2013; Hirschauer et al. 2016), other relatively massive XMPs are quite difficult to understand and challenge models of galaxy evolution (Izotov et al. 2018; McQuinn et al. 2020). These systems are strong outliers in the luminosity–metallicity and mass–metallicity relations (e.g., Mannucci et al. 2011; Berg et al. 2012; Hunt et al. 2016), with a measured metallicity far too low for their stellar mass/luminosity. Accretion of metal-poor gas either from the intergalactic medium (Filho et al. 2015) or from interaction

with smaller companions (Ekta & Chengalur 2010; McQuinn et al. 2020) is among the mechanisms proposed to explain their anomalous low metal content, but it is not always sufficient (e.g., Matteucci & Tosi 1985; Marconi et al. 1994; Pascale et al. 2022).

An iconic example of an XMP with discrepant metallicity is the nearby ($D \sim 13$ Mpc; Tikhonov et al. 2014; Sacchi et al. 2016) dwarf irregular galaxy DDO68, whose HII regions’ oxygen abundance of just $\sim 3\%$ solar (Pustilnik et al. 2005; Annibali et al. 2019) appears incompatible with its stellar mass of $M_* \sim 10^8 M_\odot$ (Sacchi et al. 2016). Although located in a void (Pustilnik & Tepliakova 2011), DDO68 has been suggested to have merged with a 10–20 times smaller gas-rich companion (named DDO68 B) responsible for its very distorted morphology characterized by a large “cometary tail” (Tikhonov et al. 2014; Sacchi et al. 2016). Deep photometry with the Hubble Space Telescope (HST) and the Large Binocular Telescope (LBT) revealed the presence of a second, even smaller ($M_* \sim 10^6 M_\odot$) interacting satellite (named S1), likely a gas-free spheroidal galaxy (Annibali et al. 2016, 2019). Consequently, DDO68 is so far the smallest dwarf galaxy with clear evidence for accretion of at least two satellites.

Pascale et al. (2022) developed detailed hydrodynamical N -body simulations of the merger of DDO68 with its two smaller satellites to reproduce the observed stellar and gaseous morphologies and the HI kinematics. They concluded that gas dilution from a 20 times smaller, metal-poor, gas-rich satellite, such as DDO68 B, is unable to explain the extremely low chemical abundances derived in DDO68; however, metallicities almost as low as the observed ones are reproduced by the simulations assuming that the companion’s accreted material has been inefficiently mixed with that of the host



Original content from this work may be used under the terms of the [Creative Commons Attribution 4.0 licence](https://creativecommons.org/licenses/by/4.0/). Any further distribution of this work must maintain attribution to the author(s) and the title of the work, journal citation and DOI.

galaxy and that the observed HII regions in fact trace the composition of the acquired satellite rather than that of DDO68's main body.

An alternative solution to the problem of the low metallicity in DDO68 was proposed by Cannon et al. (2014) based on the discovery of a candidate third interacting system in Karl Jansky Very Large Array (VLA) 21 cm observations. This gas-rich ($M_{\text{HI}} \sim 2.8 \times 10^7 M_{\odot}$) system, named DDO68 C (see Figure 1 and Table 1), lies at an angular separation of just $11'$ from DDO68, has its same systemic velocity, and appears connected to DDO68 by a low surface brightness HI bridge. These properties could indicate that the two galaxies are located at about the same distance, separated by just ~ 40 kpc in projection, and that they are gravitationally interacting. Unfortunately, both the stellar population properties and the distance of DDO68 C remain poorly constrained due to the presence of the bright foreground star TYC 1967-1114-1 (with spectral type between K0V–K2V and a magnitude of $K = 8.5$), close to the galaxy line of sight (Figures 1 and 2). This bright red interloper hampers the detection of DDO68 C from the ground in seeing-limited mode. On the other hand, GALEX far-UV (FUV) and near-UV (NUV) images, where the red foreground star is relatively faint, reveal a diffuse emission co-located with the HI detection. This suggests the presence of relatively young stars, but cannot provide direct information on the galaxy's distance. While the low surface brightness HI gas that connects DDO68 and DDO68 C offers tantalizing evidence for an ongoing interaction, a direct measurement of DDO68 C's distance would be important to place the physical association of the two systems on a more secure footing.

To make progress in understanding the nature of DDO68 C, we exploited the high spatial resolution offered by adaptive optics (AO) and acquired new deep imaging of the galaxy in the J and H bands with the SOUL+LUCI instrument on the LBT using the bright interloper star TYC 1967-1114-1 for the AO correction. This paper presents our new data capable of resolving, for the first time ever, individual stars in DDO68 C. The observations and the data reduction procedure are described in Section 2, while we present the resolved-star color–magnitude diagram (CMD) in Section 3. The discussion of the results and our conclusions are given in Section 4.

2. Observations and Data Reduction

Observations were performed at the LBT with the near-infrared LUCI camera in single conjugate adaptive optics (SCAO) mode with the second-generation AO instrument SOUL (Pinna et al. 2016, 2021). Images of DDO68 C were obtained in the J and H bands during two separate runs on 2021 January and 2021 March performing exposures of 120 s duration (8 s exposure \times 15 frames) dithered according to a rectangular pattern with $\sim 4''$ maximum displacement in the X - or Y -directions. Additional exposures were acquired at positions $\sim 40''$ off the science target for background evaluation. The AO system was correcting 500 modes at a frame rate of 1200 Hz.

The total exposure times on target, thus excluding sky observations, are 8280 s in H and 7920 s in J . The bright $K = 8.5$ mag foreground star TYC 1967-1114-1, displaced by $\sim 10''$ from DDO68 C's FUV centroid, was used for the AO correction. Observations were performed under average seeing conditions of $0''.7$ – $1''.0$. FWHMs in the AO images are in the range $\sim 0''.08$ to $\sim 0''.25$ in J and $\sim 0''.06$ to $\sim 0''.2$ in H .

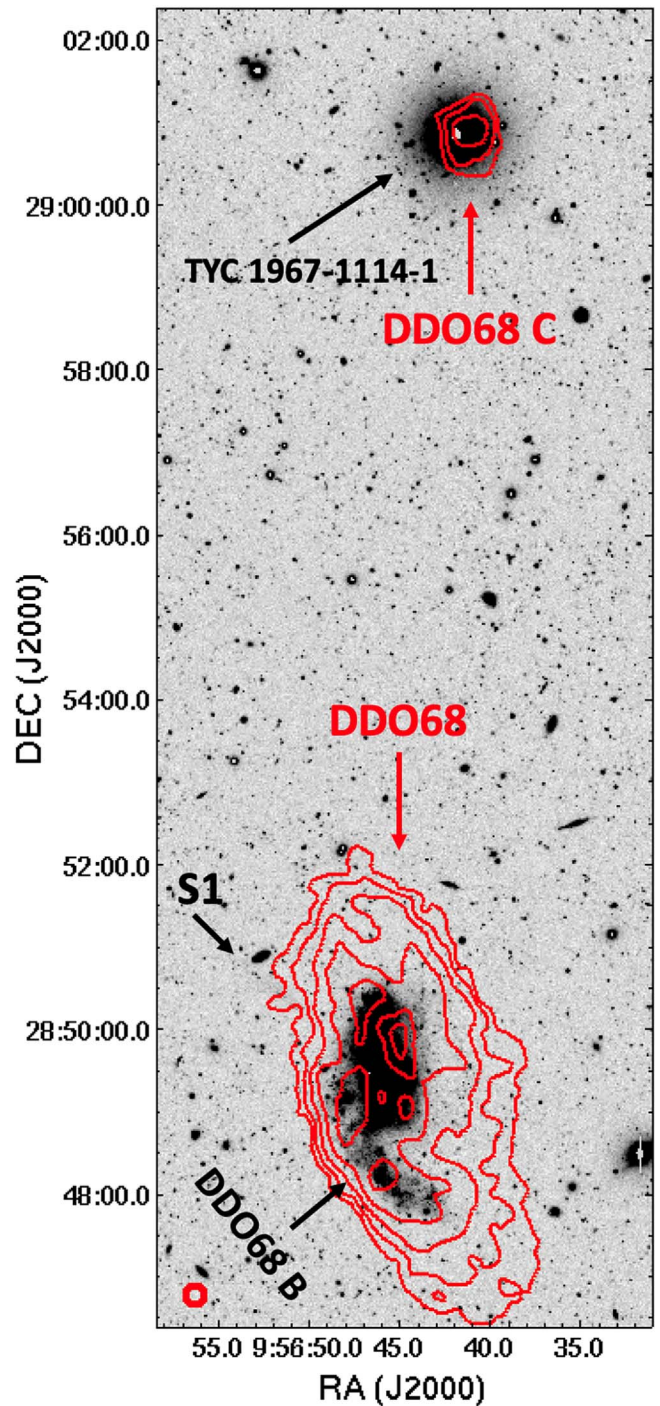


Figure 1. LBT g image of DDO68 from Annibali et al. (2016) with superimposed HI contours at $(1.25, 2.5, 5, 10, 20) \times 10^{20} \text{ cm}^{-2}$ (VLA data from Cannon et al. 2014). DDO68 C is detected in HI $\sim 11'$ north from DDO68, but is not visible in the optical because it is hidden by the bright foreground star TYC 1967-1114-1. The low surface brightness HI bridge connecting DDO68 and DDO68 C is detected in lower-resolution HI data but is not visible here. The other two confirmed satellites DDO68 B and S1 are also indicated. The $15''$ beam of the HI data is shown at the bottom left.

The individual exposures were calibrated and sky-subtracted using a dedicated pipeline developed at INAF—Rome Observatory to reduce LBT LUCI imaging data. The preliminary reduction procedure consists of removal of the dark current and of flat-field correction. The dark removal is accomplished by subtracting from each (both scientific and

Table 1
Properties of DDO68 C

Property	Value	Reference
R.A.	09 ^h 56 ^m 41. ^s 07	1
Decl.	+29° 00′ 50. [″] 74	1
Systemic velocity	~506 km s ⁻¹	1
Rotation velocity	~7.5–10 km s ⁻¹	1
Dynamical mass ^a	~10 ⁸ M _⊙	2
HI mass ^a	(2.8 ± 0.5) × 10 ⁷ M _⊙	1
SFR from FUV ^a	(1.4 ± 0.4) × 10 ⁻³ M _⊙ yr ⁻¹	1
H α luminosity ^a	<8.5 × 10 ³⁶ erg s ⁻¹	1
SFR from H α ^a	<7 × 10 ⁻⁵ M _⊙ yr ⁻¹	1
m_{FUV}	19.55 ± 0.01 [AB mag]	3
$m_{\text{FUV}} - m_{\text{NUV}}$	0.21 ± 0.06 [AB mag]	3

Notes. The last column reports the reference papers: (1) Cannon et al. (2014); (2) Pascale et al. (2022); (3) this work.

^a An assumed distance of ~13 Mpc.

sky) image a median-stacked dark image (masterdark) obtained by combining a set of dark frames acquired with the same detector integration time (DIT) and DIT number (NDIT) as the scientific data set. Each dark-subtracted image is then divided by a median-stacked flat image (masterflat) obtained through the combination of a set of dark-subtracted flat images. The prereduced science images are then sky-subtracted using a mean sky image obtained by averaging the two prereduced sky images acquired at the bounds of the temporal sequence of the scientific data set.

Since the bright foreground star TYC 1967-1114-1 used for the AO correction is outside the scientific field of view, shifts between the individual frames were computed adopting as reference the centroid of the imaged 2MASS J09563976+2900457 foreground star ($J = 13.6$, $H = 13.0$) located ~20'' west of DDO68 C (see Figure 2(e)). Upon selection of the best images with FWHM $\leq 0''.15$, individual exposures were combined into final stacked J and H deep images with total exposure times of ~3864 s and ~6944 s, respectively.

Figure 2 presents a comparison between the LUCI AO final combined image in H and the seeing-limited Sloan Digital Sky Survey (SDSS) g image, the GALEX FUV image, and the HI emission map of DDO68 C from Cannon et al. (2014). While DDO68 C is clearly identified in the FUV and HI images, the galaxy is completely outshined by the bright TYC 1967-1114-1 star in the SDSS data; on the other hand, its individual stars are well resolved in the SOUL+LUCI AO images, with the vast majority of them located in the region of the strongest UV emission. Portions of the J and H images zoomed on DDO68 C's resolved stellar component are shown in Figure 3.

Aperture photometry with the PHOT task in the IRAF environment⁵ was performed on the J and H stacked images using as input the position of sources detected above 3 times the background standard deviation in the deeper H image, and later allowing for a refined recentering of the source positions through the “centroid” option. Source fluxes were measured within a 0''.09 diameter circular aperture with the local sky evaluated in an annulus at 0''.3 radius. Aperture corrections in J

and H were evaluated from the brightest stars in DDO68 C, while the foreground star 2MASS J09563976+2900457 was used to derive photometric zero-points (see the Appendix for details). Eventually, the J and H catalogs were cross-correlated and combined into a final master catalog using the CataXcorr and CataComb routines.⁶ Spurious detections at the detector's edges and extended background galaxies were removed through visual inspection of the J and H images, providing a final catalog of ~50 bona fide stars with photometry in both bands. The photometric reduction of the LUCI AO data was repeated using SExtractor (Bertin & Arnouts 1996), including an independent estimate of the aperture corrections, in order to evaluate photometric uncertainties. The dispersion of the PHOT minus SExtractor magnitude and color difference distributions was used to infer average errors as a function of magnitude. The typical magnitude and color errors for a star as faint as $H \sim 23.75$ mag are $\sigma_H \sim 0.05$ and $\sigma_{J-H} \sim 0.13$. The derived uncertainties in different magnitude bins are shown in Figure 4.

3. Color–Magnitude Diagrams

The H , $J-H$ CMD of DDO68 C derived from the ~50 stars resolved in the LUCI images is shown in Figure 4. The CMD exhibits a sparse distribution of stars with colors in the range $0.2 \lesssim J-H \lesssim 1.4$ and magnitudes of $22 \lesssim H \lesssim 24$. The CMD does not show the typical discontinuity associated with the red giant branch (RGB) tip detection used to infer galaxy distances (Madore & Freedman 1995; Bellazzini et al. 2004). Indeed, under the assumption that DDO68 C is located at the same ~13 Mpc distance as DDO68, we would expect to detect the RGB tip at $H \gtrsim 24.5$ (the exact value depending on stellar population ages and metallicities), i.e., at least ~0.5 mag fainter than our achieved photometric depth. This is well shown in Figure 4, where we compare the observed CMD with the PARSEC+COLIBRI stellar isochrones (Bressan et al. 2012; Marigo et al. 2013; Rosenfield et al. 2016) for different ages and for two metallicity values of $Z = 0.0004$ and $Z = 0.001$ (i.e., ~2.6% and ~6.6% solar for an adopted solar value of $Z_{\odot} = 0.0152$ from Caffau et al. 2011). For an assumed 13 Mpc distance, the observed CMD is in very good agreement with the distribution of bright asymptotic giant branch (AGB) stars predicted by isochrones ~50 Myr–~2 Gyr old. Core helium-burning stars in the so-called blue loop phase, with an age of ~50 Myr, are also present. Stars older than ~2 Gyr are too faint to be detected.

For distances closer than 13 Mpc, the isochrones are shifted toward brighter magnitudes (see, e.g., panel (c) of Figure 4 for an assumed distance of ~6 Mpc). In this scenario, the CMD is poorly consistent with the stellar models, since the reddest stars with $J-H \gtrsim 1$ are incompatible with the relatively blue colors of the RGB feature, considering also the relatively low photometric uncertainty of $\sigma_{J-H} \lesssim 0.1$ mag. The observed red colors could in principle be reproduced by assuming metallicities of solar or higher, which is, however, unrealistic for the mass of DDO68 C (see Section 4) given the mass–metallicity relation of dwarf galaxies (Berg et al. 2012).

At the opposite extreme, the CMD allows us to infer upper limits on DDO68 C's distance. In panel (d) of Figure 4, the isochrones have been shifted to a distance of ~30 Mpc to

⁵ IRAF was distributed by the National Optical Astronomy Observatory, which was managed by the Association of Universities for Research in Astronomy (AURA) under a cooperative agreement with the National Science Foundation.

⁶ Part of a package of astronomical software (CataPack) developed by P. Montegriffo at INAF-OABO.

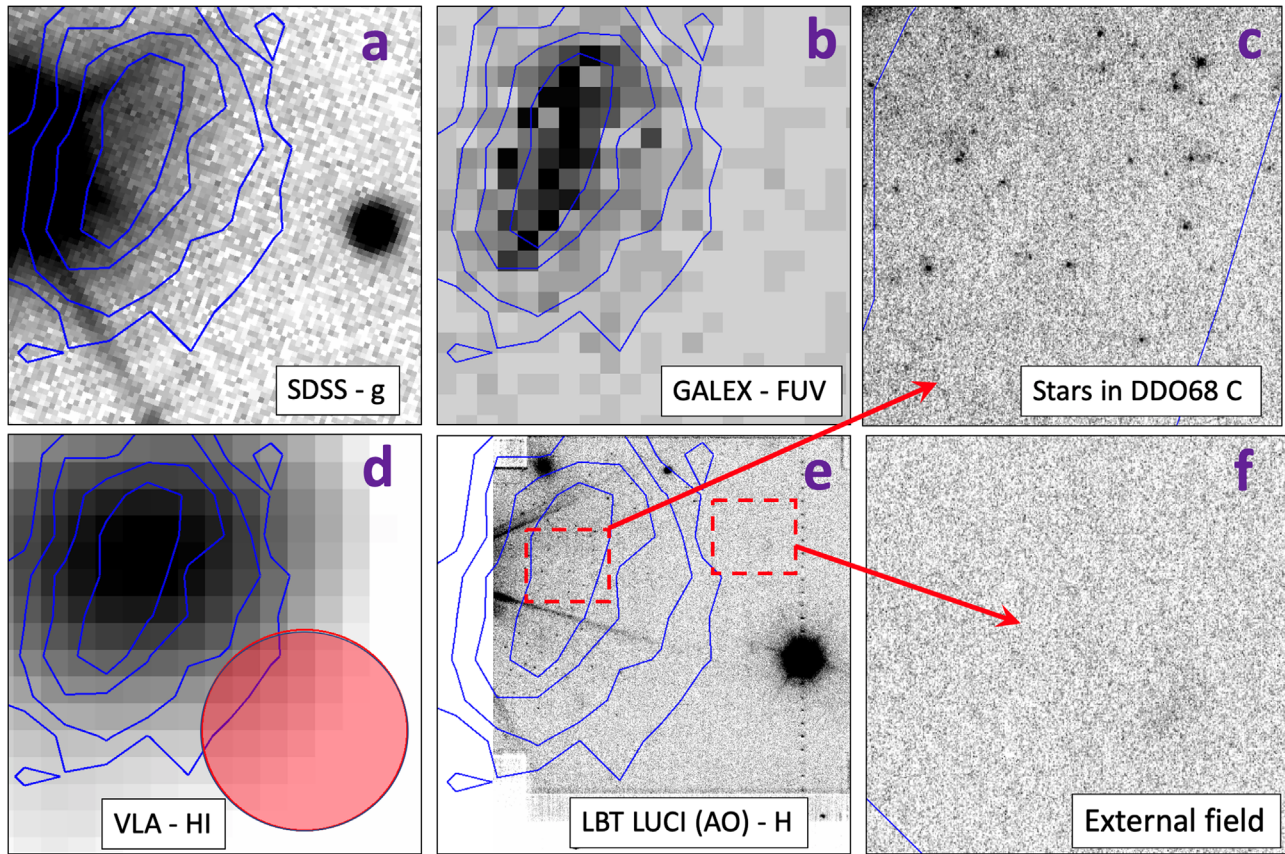


Figure 2. Images of DDO68 C in different bands: in panels (a), (b), (d), and (e) we show $30'' \times 30''$ portions of the SDSS *g* image, the GALEX FUV image, the VLA HI image (with the $15''$ beam), and the SOUL+LUCI AO *H*-band image acquired with the LBT, respectively. FUV contours at $\sim 0.3, 0.6, 1.2,$ and 2.3×10^{-15} $\text{erg s}^{-1} \text{cm}^{-2}$ are overlaid in blue on all images. In the SDSS image, the galaxy is hidden by the bright foreground red star TYC 1967-1114-1, but is visible in FUV and in HI. The bright source to the right of DDO68 C in panels (a) and (e) is the foreground star 2MASS J09563976+2900457. Panels (c) and (f) are $6'' \times 6''$ portions of the LUCI image in the *H* band centered on the stellar emission from DDO68 C and on an outer field where no stars associated with DDO68 C are detected.

match the luminosity of the 10 Myr old models with the brightest measured star. This is the youngest population (and the farthest distance) allowed for DDO68 C based on the lack of significant $\text{H}\alpha$ emission (Cannon et al. 2014), excluding a major population of ionizing stars; star formation more recent than 10 Myr ago can also be excluded based on the integrated-light FUV–NUV color, as we discuss in the next section.

4. Discussion and Conclusions

The new SOUL+LUCI AO data allowed us to resolve, for the first time ever, individual stars in the small gas-rich galaxy DDO68 C. Although the photometry is not deep enough to derive a direct distance measurement through the RGB tip method, the CMD appears fully compatible with a scenario in which the system is at the same ~ 13 Mpc distance as DDO68. Under this assumption, the comparison of the CMD with stellar evolution models reveals a population of stars with ages between ~ 50 Myr and ~ 2 Gyr, while the data are blind to older, fainter stars. Here we discuss how GALEX UV data can provide complementary information to constrain DDO68 C’s stellar populations and distance.

We downloaded GALEX *int.fits images of DDO68 C, in units of $\text{counts s}^{-1} \text{pixel}^{-1}$, from the MAST archive.⁷ Point-spread function (PSF)-fitting photometry with the DAOPHOT package (Stetson 1987) in IRAF was run to subtract the bright

foreground star TYC 1967-1114-1 in the NUV image (see Figure 5). Then aperture photometry was performed in both FUV and NUV with the IRAF POLYPHOT task within a polygonal aperture of ~ 250 arcsec^2 area encompassing the FUV contour at $\sim 0.6 \times 10^{-15}$ $\text{erg s}^{-1} \text{cm}^{-2}$ in Figure 2, enclosing the vast majority of the UV galaxy emission. Repeated flux measurements, obtained subtracting the background computed in different regions around DDO68 C, were combined to obtain average magnitudes and their standard deviations. To account for the uncertainty due to the removal of the foreground interloper in the NUV image, background values were estimated in the proximity of subtracted PSF stars. Final calibrated magnitudes in the AB system (Oke 1990) were derived through the relations $\text{FUV} = -2.5 \times \log(\text{counts s}^{-1}) + 18.82$ and $\text{NUV} = -2.5 \times \log(\text{counts s}^{-1}) + 20.08$ from the GALEX page.⁸ Foreground reddening corrections were applied adopting $E(B - V) = 0.016$ from the NED⁹ and the extinction coefficients in the GALEX filters from Yuan et al. (2013). In the end we obtain $\text{FUV} = 19.55 \pm 0.01$ mag and $\text{FUV} - \text{NUV} = 0.21 \pm 0.06$.

Figure 6 provides a comparison between the observed DDO68 C ultraviolet emission and model predictions for both simple stellar populations (SSPs) and a complex star formation history (SFH) appropriate for dwarf irregular (dIrr) galaxies.

⁷ <https://mast.stsci.edu/portal/Mashup/Clients/Mast/Portal.html>

⁸ https://asd.gsfc.nasa.gov/archive/galex/FAQ/counts_background.html

⁹ <https://ned.ipac.caltech.edu/>

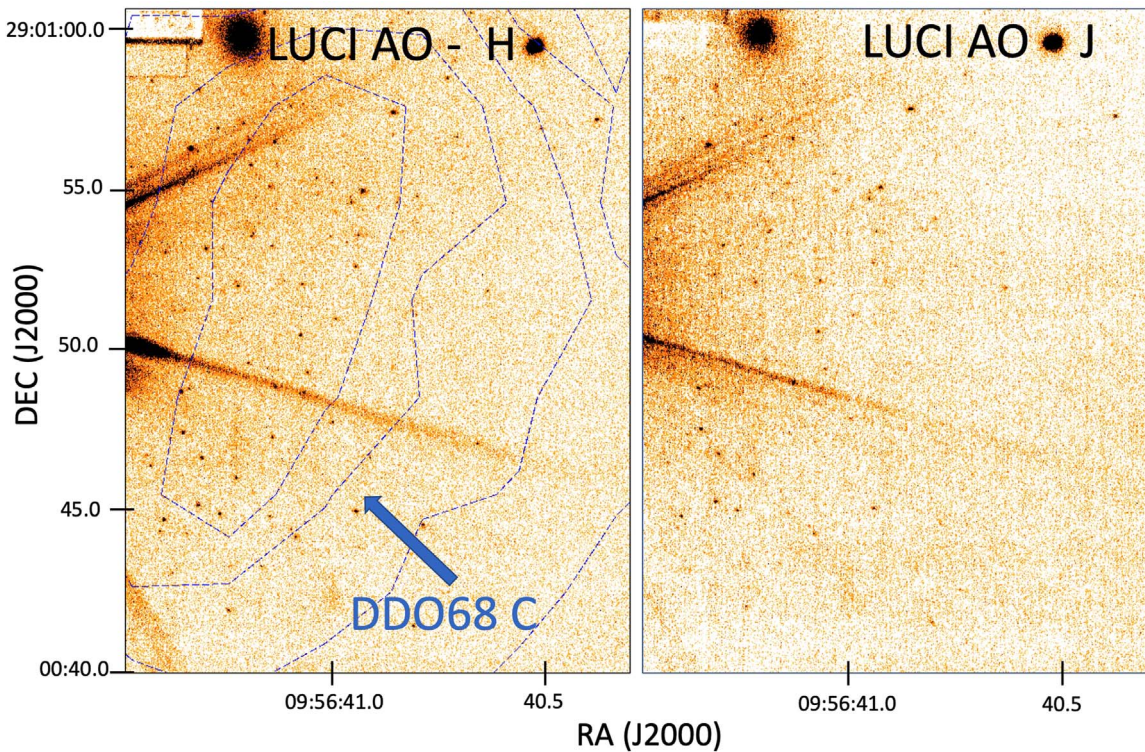


Figure 3. $15'' \times 30''$ portions of the larger SOUL+LUCI AO images of DDO68 C in the H (left) and J (right) bands capable of resolving its individual stars. Superimposed to the H image are the same GALEX FUV contours as in Figure 2. The bright foreground star TYC 1967-1114-1 used for the AO correction is outside the LUCI field of view to the east, but its prominent spikes are visible in the images. The fainter 2MASS J09563976+2900457 star used to evaluate the point-spread function and to calibrate the photometry is to the west, outside the displayed image portion.

The displayed SSPs are based on the PARSEC+COLIBRI stellar evolution models (Bressan et al. 2012; Marigo et al. 2013; Rosenfield et al. 2016) and were downloaded from the public web interface at <http://stev.oapd.inaf.it/cgi-bin/cmd>. Conversion from the models' Vegamag system to the AB system was performed through the relations $FUV(AB) = FUV(Vega) + 2.128$ and $NUV(AB) = NUV(Vega) + 1.662$ (L. Girardi, private communication). The displayed models are for a Kroupa (2001) initial mass function (IMF), for the same metallicity values of $Z = 0.0004$ and 0.001 as in Figure 4, and span ages from ~ 4 to 13 Gyr. From young to progressively older ages, the FUV luminosity decreases monotonically. At the youngest ages, the SSPs have the bluest FUV–NUV colors (of about -0.4 mag for a $Z = 0.0004$ metallicity), because O-type and B-type stars highly contribute to the FUV flux; then the FUV–NUV color increases with age due to the decreasing temperature of turnoff stars. For ages older than ~ 2 Gyr, the trend is inverted and the FUV–NUV color becomes progressively bluer due to the increased contribution from hot, post-AGB stars (see Rampazzo et al. 2011, Section 3, for a detailed discussion of the stars contributing to the FUV–NUV trend).

To account for the more complex SFH of dIrrs, we combined the PARSEC+COLIBRI SSPs according to the behavior of the median SFH derived by Weisz et al. (2014) from a sample of Local Group dIrrs with deep HST CMDs. This median SFH starts as early as ~ 13 Gyr ago and then proceeds almost continuously until present, with a typical rate that is about 2 times larger over the past ~ 4 Gyr compared to earlier epochs. Starting from the Weisz et al. (2014) SFH, we assumed quenching time to be a free parameter; in Figure 6, left panel, the values along the x -axis correspond to the epoch when star formation stopped. For a still active star formation, the

FUV–NUV color is as blue as ~ -0.1 , while a quenching occurred ~ 1 Gyr ago produces a red color of ~ 0.5 . The trend is then inverted for earlier termination epochs.

The left panel of Figure 6 shows that DDO68 C's color of $FUV-NUV = 0.21 \pm 0.06$ is compatible, within the errors and for the adopted metallicities, with an SSP age between 250 and 400 Myr. However, the CMD in Figure 4 suggests a spread in age. Under the assumption of the more complex dIrr SFH case, the UV properties of DDO68 C can be reproduced assuming quenching at ~ 60 Myr ago, a scenario also in very good agreement with the CMD of Figure 4 where the youngest populated isochrone is the 50 Myr old one. This solution provides a total stellar mass of $\sim 2 \times 10^7 M_{\odot}$ for DDO68 C, as shown in the middle panel of Figure 6. Notice that the relatively red FUV–NUV color of DDO68 C excludes the presence of current star formation, consistent both with the absence of stars younger than ~ 10 Myr in the CMD, and with the lack of significant $H\alpha$ emission (Cannon et al. 2014).

We notice in Figure 6 that the FUV–NUV color decrease for models older (or quenching epochs earlier) than 1–2 Gyr provides an alternative solution where all stars in DDO68 C are older than 2 Gyr. However, this scenario would require DDO68 C to lie at a much closer distance of ~ 6 Mpc in order for the brightest resolved stars in the CMD to be compatible with the maximum luminosity of the ~ 2 Gyr old stellar isochrones, as illustrated in Figure 4(c). We show in the right panel of Figure 6 that this scenario is compatible with the observed FUV and NUV galaxy magnitudes if a total stellar mass of $\sim 2 \times 10^7 M_{\odot}$ is assumed. However, at a 6 Mpc distance, this mass should have formed within a 0.21 kpc^2 region, implying an average stellar mass density of $\Sigma_{*} \sim 100 M_{\odot} \text{ pc}^{-2}$, which appears unrealistically high compared to

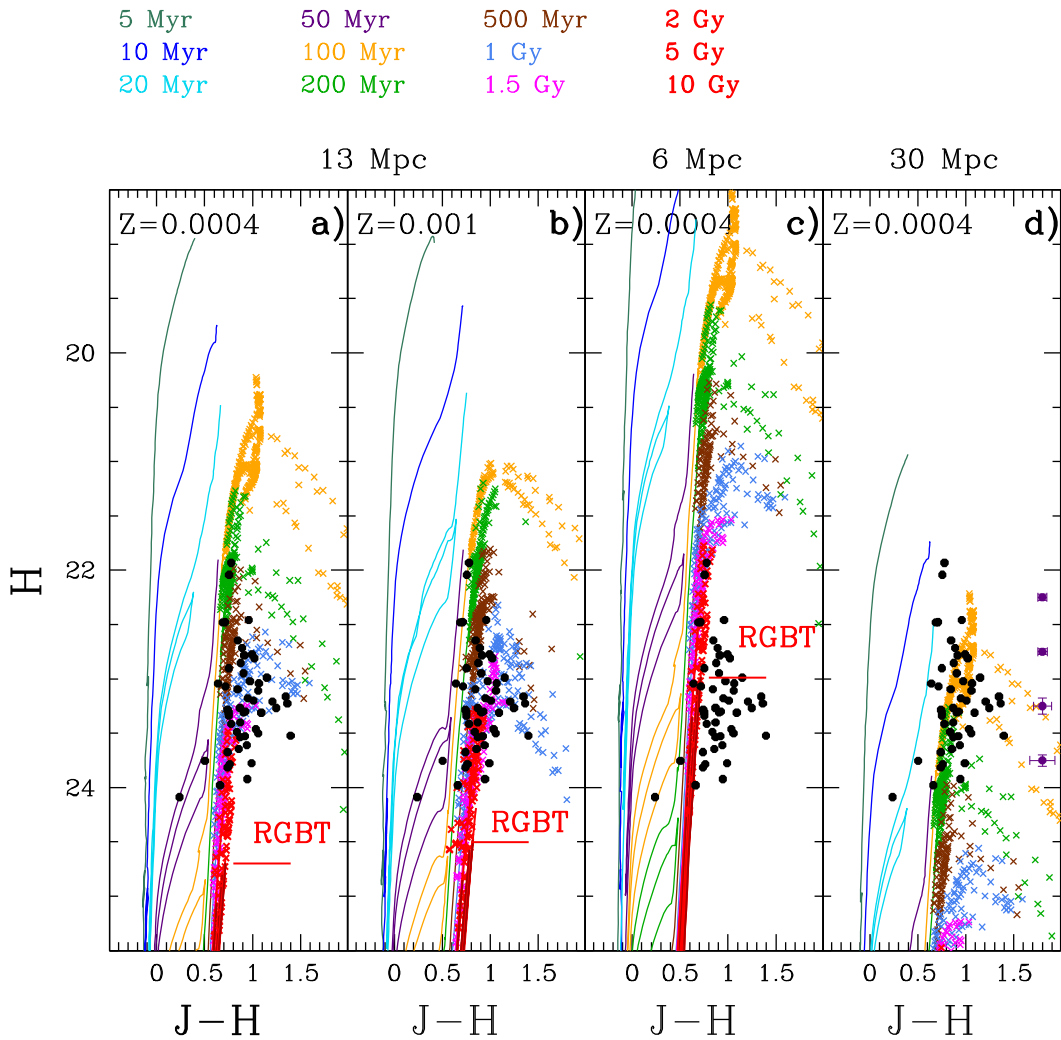


Figure 4. H vs. $J-H$ CMD of stars (black dots) resolved in DDO68 C with LUCI AO. Superimposed as crosses with different colors, as indicated in the legend, are the PARSEC+COLIBRI stellar isochrones (Bressan et al. 2012; Marigo et al. 2013; Rosenfield et al. 2016) for different ages and for metallicities of $Z = 0.0004$ ($\sim 2.6\%$ solar) and $Z = 0.001$ ($\sim 6.6\%$ solar) shifted to DDO68’s distance of ~ 13 Mpc (panels (a) and (b)). At that distance, the photometry is compatible with stars ~ 50 Myr to ~ 2 Gyr old. Stars older than ~ 2 Gyr are too faint to be detected, with the expected magnitude of the RGB tip (RGBT) indicated by the horizontal segment. Panels (c) and (d) provide a comparison of the observed CMD with isochrones shifted to distances of 6 Mpc and 30 Mpc, respectively. Typical photometric errors in H and $J-H$ as a function of magnitude are shown in the lower right portion of panel (d).

values derived in other dIrrs (e.g., Sacchi et al. 2016; McQuinn et al. 2021).

At the opposite extreme, we explored a scenario in which DDO68 C lies at a much larger distance of ~ 30 Mpc, the maximum distance allowed by the brightest resolved star in the CMD of Figure 4 given the lack of significant $H\alpha$ emission, thus of ionizing stars younger than ~ 10 Myr. According to the models in the right panel of Figure 6, the galaxy stellar mass would be, in this case, as high as $\sim 10^8 M_\odot$, potentially close to the galaxy dynamical mass. In addition, the relatively red FUV–NUV color of DDO68 C appears incompatible with the presence of stars as young as 10 Myr, which would produce typically bluer colors.

In conclusion, the combined analysis of the SOUL+LUCI AO resolved-star photometry, archival GALEX data, and $H\alpha$ images from Cannon et al. (2014) support a scenario in which DDO68 C has been actively forming stars in the past (possibly since ~ 13 Gyr ago, as in Local Group dIrrs) but has quenched (or significantly suppressed) its activity about 50–60 Myr ago. All data, including the systemic HI velocity derived by Cannon et al. (2014), are best reproduced by the assumption that

DDO68 C is at the same ~ 13 Mpc distance as its candidate interacting companion DDO68. In fact, although the new AO data do not provide a direct distance measurement to DDO68 C through the RGB tip method (which would require the superb depth and spatial resolution of HST or JWST), the assumption of alternative distances tend to produce either a mismatch between the resolved-star CMD and stellar isochrones, and/or unrealistically high stellar mass or stellar mass density, and/or major inconsistency between the UV properties of DDO68 C and predictions from population synthesis models.

The proposed scenario in which DDO68 C, DDO68 B, and S1 are all satellites of DDO68 puts new constraints on theoretical predictions on the number of satellites around isolated dwarf galaxies with the mass of DDO68. For instance, some cosmological N -body simulations coupled with abundance matching models foresee at most one luminous satellite more massive than $M_* \sim 10^6 M_\odot$ around a host with the mass of DDO68 (Dooley et al. 2017; Santos-Santos et al. 2022). DDO68 is indeed the only case so far of a low-mass dwarf (less massive than the Magellanic Clouds) known to be interacting with three smaller systems, a peculiarity that offers tantalizing

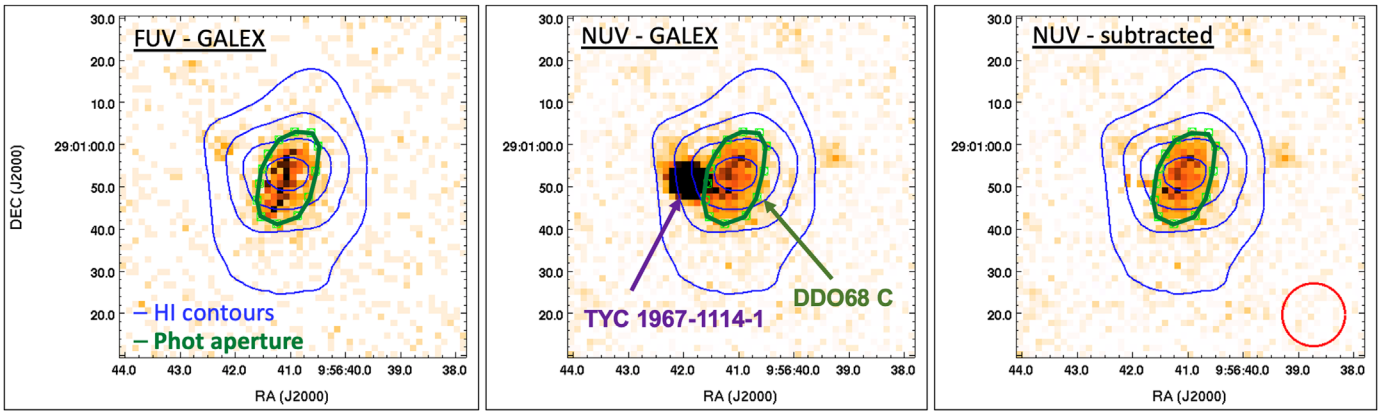


Figure 5. GALEX FUV and NUV images of DDO68 C with a field of view of $80'' \times 80''$. Superimposed in blue, thin curves, are the HI contours at (2, 4, 6, 8) $\times 10^{20} \text{ cm}^{-2}$ from the same data of Cannon et al. (2014). The thicker green polygon is the aperture used to compute the FUV and NUV magnitudes. The bright foreground star TYC 1967-1114-1, well visible in the NUV central panel, was subtracted in the rightmost panel before computing the galaxy NUV emission. Here the circle denotes the $15''$ beam of the HI data.

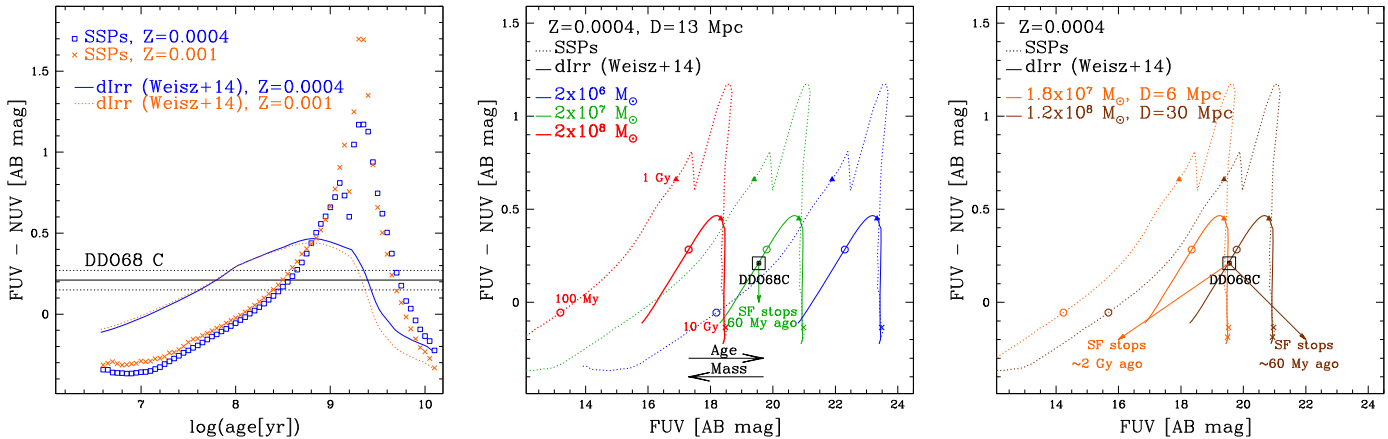


Figure 6. Left: predicted FUV–NUV GALEX colors in the AB mag system as a function of stellar age for simple stellar populations (SSPs, open symbols) generated from the PARSEC+COLIBRI models for a Kroupa (2001) IMF and for two metallicities of $Z = 0.0004$ and $Z = 0.001$. The solid and dashed curves correspond instead to a typical dlrr SFH (Weisz et al. 2014) with the assumption of different quenching epochs, indicated in the x-axis (see the text for details). The horizontal lines denote the average color and associated uncertainty for DDO68 C. Middle: same models (only for $Z = 0.0004$) in the FUV–NUV vs. FUV plane, assuming a distance of 13 Mpc and different stellar masses of 2×10^6 , 2×10^7 , and $2 \times 10^8 M_{\odot}$. Along each model, age increases from left to right. The observed values for DDO68 C (notice that the uncertainties are smaller than the symbol size) are compatible with a dlrr SFH assuming quenching at about ~ 60 Myr ago and a total galaxy stellar mass of $\sim 2 \times 10^7 M_{\odot}$. Right: two alternative solutions, with distances of 6 Mpc and 30 Mpc, stellar masses of $\sim 2 \times 10^7$ and $\sim 1 \times 10^8 M_{\odot}$, and quenching epochs at ~ 2 Gyr and ~ 60 Myr ago, respectively, are also compatible with the GALEX magnitudes of DDO68 C.

explanation for its anomalous extremely low metallicity. Although the actual gas mass of DDO68 C equals just few percent of the gas mass in DDO68, thus insufficient to dilute the gas to the extremely low metallicity observed (Pascale et al. 2022), it may have been higher in the past before being deposited into its more massive companion. Deeper data on the diffuse gas connecting the two systems as well as more accurate dynamical mass estimates for DDO68 C would be crucial to better constrain hydrodynamical N -body simulations for the merging history of DDO68 with its satellites’ population.

We thank L. Girardi for his precious support with the PARSEC+COLIBRI stellar models. We are grateful to the anonymous referee for the constructive report that helped to improve the paper. We acknowledge the support from the LBT-Italian Coordination Facility for the execution of observations, data distribution, and reduction. F.A., M.B., R.P., and M.T. acknowledge the financial support from INAF Main Stream grant

1.05.01.86.28 “SSH.” F. A., L.K.H., and M.T. acknowledge funding from INAF PRIN-SKA-2017 program 1.05.01.88.04. R.P. acknowledges support from PRIN INAF 1.05.01.85.01.

Based on data acquired using the Large Binocular Telescope (LBT). The LBT is an international collaboration among institutions in the United States, Italy, and Germany. LBT Corporation partners are The University of Arizona on behalf of the Arizona university system; Istituto Nazionale di Astrofisica, Italy; LBT Beteiligungsgesellschaft, Germany, representing the Max-Planck Society, the Astrophysical Institute Potsdam, and Heidelberg University; The Ohio State University; and The Research Corporation, on behalf of The University of Notre Dame, University of Minnesota, and University of Virginia.

This research has made use of the SIMBAD database, operated at CDS, Strasbourg, France. This research has made use of the NASA/IPAC Extragalactic Database (NED) which is operated by the Jet Propulsion Laboratory, California Institute of Technology, under contract with the National

Aeronautics and Space Administration. This research has made use of NASA's Astrophysics Data System.

Facilities: LBT(SOUL+LUCI), GALEX.

Software: SExtractor (Bertin & Arnouts 1996), DAOPHOT (Stetson 1987).

Appendix

Spatially Variable Aperture Corrections and Photometric Zero-points

Photometric calibration in the J and H bands for stars in DDO68 C was performed according to the formula

$$J, H_{\text{cal}} = J, H_6 + AC_{J,H} + ZP_{J,H}, \quad (\text{A1})$$

where J, H_{cal} are the calibrated magnitudes, J, H_6 are the instrumental magnitudes derived from aperture photometry within the adopted 6 pixel ($0''.09$) diameter aperture, $AC_{J,H}$ are the aperture corrections to a larger $5 \times \text{FWHM}$ aperture (enclosing $\sim 80\%$ of the total flux), and $ZP_{J,H}$ are the photometric zero-points in the two bands.

The variation of the shape of the PSF with increasing distance from the AO star (e.g., Wilson & Jenkins 1996) requires in fact the implementation of a spatially variable aperture correction. Indeed, for the bright foreground star 2MASS J09563976+2900457, at $\sim 30''$ distance from the AO star, we measure a PSF FWHM $\sim 0''.15$ in J and $\sim 0''.12$ in H ; on the other hand, stars belonging to DDO68 C at $\sim 10''$ distance from the AO star have FWHM $\sim 0''.07$ in J and $\sim 0''.06$ in H . Notice that the larger PSF derived in J reflects the typically worse atmospheric conditions during observations in this band.

Aperture corrections were computed selecting the brightest ($H \lesssim 23$) and most isolated stars in the observed field, paying attention to remove sources on top of prominent AO star spikes. We ended up with a sample of 11 stars, for which photometry was computed within a larger diameter aperture of 5 times the FWHM (i.e., $0''.35$ or 23 pixels in J and $0''.3$ or 20 pixels in H), chosen to capture the largest possible fraction of the total flux while minimizing contamination from background noise. Figure 7 shows the behavior of the J and H aperture corrections (computed as the difference between the 20 or 23 pixel aperture photometry and the 6 pixel aperture photometry) as a function of distance from the AO star. As expected, these corrections increase (in absolute value) with distance from the AO star due to the increase in the PSF FWHM. However, because of the similar slopes of the relations in J and H , the trend on the combined $J-H$ color is flat, as shown in the bottom panel of Figure 7.

Least-squares linear fits to the data points provide the following relations for the spatially variable aperture corrections:

$$AC_J = \text{mag}_{J,5\text{FWHM}} - \text{mag}_{J,6} = -0.04 \times D_{\text{AO}} - 0.8, \quad (\text{A2})$$

$$AC_H = \text{mag}_{H,5\text{FWHM}} - \text{mag}_{H,6} = -0.04 \times D_{\text{AO}} - 0.6, \quad (\text{A3})$$

where D_{AO} is the distance from the AO star in arcsec. For each star in DDO68 C, aperture corrections were then calculated injecting its AO star distance into Equations (A2) and (A3).

Photometric zero-points were derived using the bright foreground star 2MASS J09563976+2900457, with total magnitudes of $J = 13.60 \pm 0.02$ and $H = 13.00 \pm 0.03$ from Skrutskie et al. (2006). Photometry in J and H was then performed for this star from our images within diameter

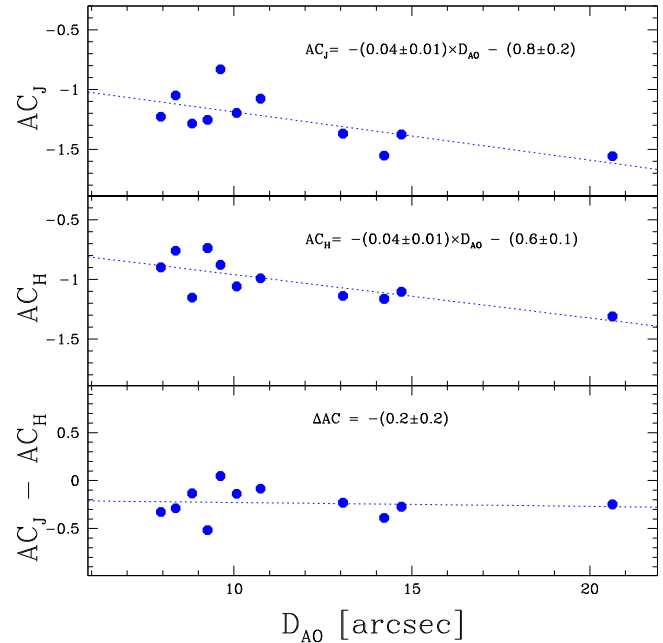


Figure 7. Aperture corrections in J (AC_J) and H (AC_H) as a function of distance from the AO star derived from the brightest and most isolated stars in DDO68 C. The corrections were computed as the magnitude difference at apertures of 20/23 pixels (i.e., 5 times the FWHM at $\sim 10''$) and 6 pixels. The bottom panel displays the difference between the J and H aperture corrections, showing no significant trend with distance from the AO star. Dotted lines are the least-squares linear fits.

apertures of $0''.75$ and $0''.6$ in J and H , respectively (i.e., 5 times its FWHM), in order to properly tie the zero-points to the aperture corrections provided by Equations (A2) and (A3).

The derived zero-points are

$$ZP_J = J_{2\text{MASS}} - J_{5\text{FWHM}} = 28.32, \quad (\text{A4})$$

$$ZP_H = H_{2\text{MASS}} - H_{5\text{FWHM}} = 28.03. \quad (\text{A5})$$

The uncertainties in the overall photometric calibration are of order 0.1–0.2 mag (see the uncertainties associated with the zero-points of the relations in Figure 7), and they do not significantly change our conclusions.

ORCID iDs

Leslie K. Hunt <https://orcid.org/0000-0001-9162-2371>
 Diego Paris <https://orcid.org/0000-0002-7409-8114>
 Felice Cusano <https://orcid.org/0000-0003-2910-6565>
 Michele Bellazzini <https://orcid.org/0000-0001-8200-810X>
 John M. Cannon <https://orcid.org/0000-0002-1821-7019>
 Monica Tosi <https://orcid.org/0000-0002-0986-4759>

References

- Annibali, F., Bellazzini, M., Correnti, M., et al. 2019, *ApJ*, 883, 19
 Annibali, F., La Torre, V., Tosi, M., et al. 2019, *MNRAS*, 482, 3892
 Annibali, F., Nipoti, C., Ciotti, L., et al. 2016, *ApJL*, 826, L27
 Annibali, F., & Tosi, M. 2022, *NatAs*, 6, 48
 Bellazzini, M., Ferraro, F. R., Sollima, A., et al. 2004, *A&A*, 424, 199
 Berg, D. A., Skillman, E. D., Marble, A. R., et al. 2012, *ApJ*, 754, 98
 Bertin, E., & Arnouts, S. 1996, *A&AS*, 117, 393
 Bressan, A., Marigo, P., Girardi, L., et al. 2012, *MNRAS*, 427, 127
 Caffau, E., Ludwig, H.-G., Steffen, M., et al. 2011, *SoPh*, 268, 255
 Cannon, J. M., Johnson, M., McQuinn, K. B. W., et al. 2014, *ApJL*, 787, L1
 Dooley, G. A., Peter, A. H. G., Yang, T., et al. 2017, *MNRAS*, 471, 4894
 Ekta, B., & Chengalur, J. N. 2010, *MNRAS*, 406, 1238
 Filho, M. E., Sánchez Almeida, J., Muñoz-Tuñón, C., et al. 2015, *ApJ*, 802, 82
 Guseva, N. G., Izotov, Y. I., Fricke, K. J., et al. 2015, *A&A*, 579, A11

- Guseva, N. G., Izotov, Y. I., Fricke, K. J., et al. 2017, *A&A*, **599**, A65
- Hirschauer, A. S., Salzer, J. J., Skillman, E. D., et al. 2016, *ApJ*, **822**, 108
- Hsyu, T., Cooke, R. J., Prochaska, J. X., et al. 2017, *ApJL*, **845**, L22
- Hsyu, T., Cooke, R. J., Prochaska, J. X., et al. 2018, *ApJ*, **863**, 134
- Hunt, L., Dayal, P., Magrini, L., & Ferrara, A. 2016, *MNRAS*, **463**, 2002
- Izotov, Y. I., Thuan, T. X., & Guseva, N. G. 2012, *A&A*, **546**, A122
- Izotov, Y. I., Thuan, T. X., Guseva, N. G., & Liss, S. E. 2018, *MNRAS*, **473**, 1956
- Izotov, Y. I., Thuan, T. X., & Lipovetsky, V. A. 1994, *ApJ*, **435**, 647
- Kojima, T., Ouchi, M., Rauch, M., et al. 2020, *ApJ*, **898**, 142
- Kroupa, P. 2001, *MNRAS*, **322**, 231
- Kunth, D., & Östlin, G. 2000, *A&ARv*, **10**, 1
- Madore, B. F., & Freedman, W. L. 1995, *AJ*, **109**, 1645
- Mannucci, F., Salvaterra, R., & Campisi, M. A. 2011, *MNRAS*, **414**, 1263
- Marconi, G., Matteucci, F., & Tosi, M. 1994, *MNRAS*, **270**, 35
- Marigo, P., Bressan, A., Nanni, A., Girardi, L., & Pumo, M. L. 2013, *MNRAS*, **434**, 488
- Matteucci, F., & Tosi, M. 1985, *MNRAS*, **217**, 391
- McQuinn, K. B. W., Berg, D. A., Skillman, E. D., et al. 2020, *ApJ*, **891**, 181
- McQuinn, K. B. W., Telidevara, A. K., Fuson, J., et al. 2021, *ApJ*, **918**, 23
- Oke, J. B. 1990, *AJ*, **99**, 1621
- Pascale, R., Annibali, F., Tosi, M., et al. 2022, *MNRAS*, **509**, 2940
- Pinna, E., Esposito, S., Hinz, P., et al. 2016, *Proc. SPIE*, **9909**, 99093V
- Pinna, E., Rossi, F., Puglisi, A., et al. 2021, arXiv:2101.07091
- Pustilnik, S. A., Egorova, E. S., Kniazev, A. Y., et al. 2021, *MNRAS*, **507**, 944
- Pustilnik, S. A., Kniazev, A. Y., & Pramskij, A. G. 2005, *A&A*, **443**, 91
- Pustilnik, S. A., & Tepliakova, A. L. 2011, *MNRAS*, **415**, 1188
- Rampazzo, R., Annibali, F., Marino, A., et al. 2011, *Ap&SS*, **335**, 201
- Rosenfield, P., Marigo, P., Girardi, L., et al. 2016, *ApJ*, **822**, 73
- Sacchi, E., Annibali, F., Cignoni, M., et al. 2016, *ApJ*, **830**, 3
- Santos-Santos, I. M. E., Sales, L. V., Fattahi, A., & Navarro, J. F. 2022, *MNRAS*, **515**, 3685
- Senchyna, P., Stark, D. P., Chevillard, J., et al. 2019, *MNRAS*, **488**, 3492
- Skillman, E. D., Salzer, J. J., Berg, D. A., et al. 2013, *AJ*, **146**, 3
- Skrutskie, M. F., Cutri, R. M., Stiening, R., et al. 2006, *AJ*, **131**, 1163
- Stetson, P. B. 1987, *PASP*, **99**, 191
- Tikhonov, N. A., Galazutdinova, O. A., & Lebedev, V. S. 2014, *AstL*, **40**, 1
- Weisz, D. R., Dolphin, A. E., Skillman, E. D., et al. 2014, *ApJ*, **789**, 147
- Wilson, R. W., & Jenkins, C. R. 1996, *MNRAS*, **278**, 39
- Yang, H., Malhotra, S., Rhoads, J. E., et al. 2017, *ApJ*, **847**, 38
- Yuan, H. B., Liu, X. W., & Xiang, M. S. 2013, *MNRAS*, **430**, 2188